sustainability

MDPI

Article

Investigation of Structural, Magnetic, Optical, and Photocatalytic Properties of Fe/$CoFe_2O_4$ Composite

Liliya Frolova [1,*], Vyacheslav Protsenko [2] and Tetiana Butyrina [1]

[1] Department of Inorganic Materials Technology and Ecology, Ukrainian State University of Science and Technologies, 49010 Dnipro, Ukraine
[2] Department of Physical Chemistry, Ukrainian State University of Science and Technologies, 49010 Dnipro, Ukraine
* Correspondence: 19kozak83@gmail.com

Abstract

A Fe/$CoFe_2O_4$ nanocomposite was synthesized in one step by a hydrothermal method by processing the created iron and cobalt hydroxocomplexes. For precise characterization of the structure and morphology, X-ray diffraction (XRD), Fourier transform infrared spectroscopy, scanning electron microscopy, and ultraviolet–visible diffuse reflectance spectroscopy (UV-vis-DRS) were used. It was found that the obtained samples have a pronounced spinel crystalline structure, with the presence of metallic iron. The crystal size was determined by various methods and was 93–104 nm. The saturation magnetization, determined from the hysteresis loop, was 189.24 Emu/g, and the force coefficient was 602 Oe. UV-vis-DRS studies showed a band gap of 2.1 eV. The photocatalytic degradation of ibuprofen, streptocide, furacilin, methylene blue, and tetracycline was investigated under the influence of UV radiation in the presence of a photocatalyst. It was confirmed that the rate of degradation of pollutants obeys pseudo-first-order kinetics. Analysis of the constant rate of reactions showed that in order of decreasing stability, pharmaceutical drugs can be dissolved as follows: ibuprofen → streptocide → furatsilin → methylene blue → tetracycline. It was found that the ratio of photocatalyst and hydrogen peroxide concentrations is important for the destruction of more stable pollutants. The effect of hydrogen peroxide and catalyst concentrations is extremely strong. For unstable compounds, the most influential factor is the duration of treatment.

Keywords: composite; saturation magnetization; coercive force; crystallites

Academic Editor: Konstantinos S. Triantafyllidis

Received: 27 October 2025
Revised: 14 November 2025
Accepted: 17 November 2025
Published: 20 November 2025

Citation: Frolova, L.; Protsenko, V.; Butyrina, T. Investigation of Structural, Magnetic, Optical, and Photocatalytic Properties of Fe/$CoFe_2O_4$ Composite. *Sustainability* **2025**, *17*, 10415. https://doi.org/10.3390/su172210415

1. Introduction

At present, the interest of scientists in the treatment of wastewater from pharmaceuticals (PPs) is growing, as sustainable development requires a balance between economic growth, environmental protection, and human health, and the pollution of water bodies with PPs threatens all three. Active pharmaceutical ingredients (APIs) have recently been identified as pollutants of increasing concern that are potentially hazardous to the environment and human health, but most are currently not subject to environmental regulation [1]. The stability and biological activity of these highly water-soluble contaminants, which occur in micromolar concentrations, can lead to the development of resistance and other health-related effects. Research into the impact of pharmaceuticals primarily focuses on their prevalence in surface waters and hydrosphere pollution. Typically, drugs that are widely used in medicine, persistent in aquatic environments, and ineffectively removed

by water treatment systems are studied in detail [1]. The occurrence of pharmaceuticals in an urban alluvial aquifer was investigated, and their risk to human health was assessed. The results showed that 35 pharmaceuticals, including 6 transformation products, were detected in all groundwater samples, and the concentrations ranged from low to μg/L [2]. A study [3] investigated the occurrence, distribution, and potential sources of 34 pharmaceuticals and personal care products in water, sediment, aquatic organisms (fish and shellfish), and fish feed from mariculture areas of the Pearl River Delta. Spectinomycin, paracetamol, ciprofloxacin, norfloxacin, and ibuprofen were the most frequently detected in feed. Ibuprofen and ketoprofen were widely detected in aquatic organisms, with average concentrations of 562 and 267 ng/g wet weight, respectively.

Antimicrobial resistance in bacterial pathogens is a serious problem that leads to high morbidity and mortality. Multidrug resistance of Gram-positive and Gram-negative bacteria is difficult to treat and may even be untreatable with traditional drugs. For example, ibuprofen is mentioned as being on the list of priority pharmaceutical contaminants [4]; tetracycline is also on the list of priority pollutants in Denmark, while ibuprofen, tetracycline, and furatsilin are found in water bodies worldwide [5].

Although the concentration of pharmaceuticals decreases over time due to partial destruction, filtration through aquifers, adsorption, and oxidation–reduction reactions, it is necessary to develop effective wastewater treatment methods.

Standard treatment facilities do not completely remove pharmaceuticals because they are stable and soluble, so additional methods are necessary. The development of industrial wastewater treatment technologies is of great importance. Advanced oxidation processes (AOPs), including ozonation, UV radiation, electrolysis, and photocatalysis, play a key role [4,6]. AOPs generate various reactive species, including non-selective OH radicals, which promote the degradation of a wide range of organic compounds. The Fenton reaction is characterized by high mineralization efficiency and is inexpensive, simple, and environmentally friendly [5,7]. The classic version of the Fenton process requires the use of acidic solutions, which necessitates additional treatment. In addition, homogeneous catalysis leads to secondary contamination with iron(II) and iron(III) cations, which is unacceptable.

The use of the heterogeneous photo-Fenton process, which utilizes metal hydroxides, oxides, and oxyhydroxides as catalysts, significantly expands the potential for water treatment. Unlike homogeneous catalysis, heterogeneous catalysis is effective over a wide pH range and reaches its maximum efficiency when used [6–11].

Currently, numerous studies are devoted to the development of new photocatalysts [12–14], including ferrite ones, with high stability and activity for the degradation of pharmaceuticals [10–12,15–17].

Ferrite-based composites typically exhibit excellent performance due to their multifunctionality and magnetic separation capabilities [18,19]. These materials provide high adsorption efficiency and fast kinetics for the removal of pollutants such as metal ions, dyes, and pharmaceuticals [20–24].

Nanocomposites of spinel ferrites with carbon materials have been shown to exhibit strong photocatalytic activity in the degradation of pollutants [25,26]. For example, nickel ferrite-based composites have been studied for water purification from organic pollutants [27]. They are effective in removing a wide range of pollutants that are present in water, such as dyes such as methylene blue, rhodamine B, methyl orange, Congo red, and antibiotics (tetracycline, oxytetracycline, ampicillin, and sulfamethoxazole).

Reference [28] describes the synthesis of nickel ferrite (NiFe) nanoparticles, nitrogen-doped mesoporous carbon nanoflakes (NCF), and a novel nickel ferrite–carbon nanoflake nanocomposite (NiFe@NCF) using a solvothermal method. The synthesized nanoparti-

cles were used as a heterogeneous photocatalyst for the degradation of water pollutants: ciprofloxacin (CIP) and levofloxacin (LEV). A total of 99.91% of LEV and 98.86% of CIP were degraded within 50 and 70 min under visible-light irradiation using NiFe@NCF according to pseudo-first-order kinetics. The increased efficiency of the nanocomposite is due to the larger surface area, a decrease in the band gap (from 2.42 to 2.19 eV), a large number of active centers, and the mobility of charge carriers.

The use of TiO_2-$CoFe_2O_4$ and TiO_2-$CuFe_2O_4$ composite films exhibited excellent performance in the photocatalytic degradation of indigo carmine as a model dye at pH 3 under the action of UV and visible radiation [29].

An extremely efficient and highly adaptive photocatalyst, La-$CuFe_2O_4$/g-C_3N_4 (LCFO/CN), was obtained using the hydrothermal method [30].

The efficiency of the photocatalyst (lanthanum-doped copper ferrite/graphitic carbon nitride composites) was tested using the dye rhodamine B (RhB). The composite's degradation rate was 97.35% due to an increased surface area, an increased number of active sites, and a decreased band gap compared to the components [31].

Ternary hybrid composites of $Ni_{0.5}Zn_{0.5}Fe_2O_4/CeO_2$ and $Ni_{0.5}Zn_{0.5}Fe_2O_4/CeO_2$/multiwalled carbon nanotube (MWCNT) nanocomposites exhibit excellent photocatalytic degradation efficiency (93.5%) for the removal of rose bengal (RB) dye from wastewater under UV radiation [32].

A detailed analysis of ferrites and their nanocomposites revealed the influence of various parameters, such as substrate concentration, solution pH, photocatalyst amount, photocatalyst surface area, metal and non-metal ion doping, light intensity, and irradiation time, on the photocatalytic degradation of organic wastewater [33,34].

Despite a large number of review articles, little research has been devoted to the degradation of pharmaceuticals. Therefore, the synthesis of new composite photocatalysts and the study of their photocatalytic properties for the degradation of the aforementioned pollutants are of paramount importance.

The aim of this study is to obtain a Fe/$CoFe_2O_4$ composite by coprecipitation and hydrothermal treatment, as well as to investigate its physicochemical properties and photocatalytic activity in the degradation of pharmaceuticals with different chemical structures but belonging to a group of pharmaceutically active compounds.

2. Materials and Methods

$FeSO_4 \times 7H_2O$, $CoSO_4 \times 7H_2O$, and sodium hydroxide were used in the experiments. All substances were provided by Khimlaborreaktiv LLC (Ukraine) and were of a chemically pure grade without additional purification. All solutions were prepared using distilled water. $FeSO_4$ and $CoSO_4$ solutions were mixed with an iron to a cobalt cation molar ratio of 2:1. A 1 M NaOH solution was then slowly added to the resulting solution, and the pH of the solution was adjusted to 12. In the next step, the resulting colloidal solution was poured into a 300 mL Teflon beaker, which was then kept in a steel autoclave at 250 °C for 4 h.

The phase composition of the samples was studied using a DRON-2.0 diffractometer with Co-K_a radiation (JSC "Bourevestnik", Saint Petersburg, Russia). The operating mode of the X-ray source is 40 kV, 30 mA. The scanning angle range 2θ is from 10 to 90°. A JSM-6390LV scanning electron microscope (JEOL Ltd., Tokyo, Japan) was used to study the morphology of the samples.

The magnetic properties of the samples were determined from the magnetic hysteresis loop, obtained by vibration magnetometry. To study the absorption of electromagnetic waves, samples were prepared in the form of films. The composite material was uniformly mixed in polyvinyl alcohol with a loading of 20% by weight. Fourier transform infrared

spectra were obtained in the wavenumber range of 400–4000 cm^{-1} using a Spectrum One spectrophotometer (Shelton, CT, USA) in KBr tablets at 25 °C.

Photocatalytic properties were obtained using a model of methylene blue, furatsilin, tetracycline, streptocide, and ibuprofen. Experiments on the catalytic decomposition of MB were conducted in a glass vessel at 25 °C with constant shaking. A DKB 9 UV lamp (Lisma, Saransk, Russia) with an effective spectral range of 180–275 nm was used as the irradiation source. The UV radiation intensity was approximately 3 mW/cm^2. The lamp was positioned 10 cm above the solution. Before adding the catalyst, the maximum absorbance of the model solution was measured using a UV-5800 PC spectrophotometer (Metash Instruments, Shanghai, China). in the 200–900 nm range.

To assess the influence of selected factors, the method of central composite experimental design was used. The influence of parameters such as photocatalyst concentration (X_1), volume of H_2O_2 (X_2), and UV irradiation time (X_3) on the degradation of methylene blue, furatsilin, tetracycline, streptocide, and ibuprofen was determined. The core of the central composite design was a full factorial experiment (FFE) of the n = 3 type.

The FFE plan was supplemented with a certain number of star points, the coordinates of which depend on the adopted optimality principle. The total number of experiments with this planning is determined by Formula (1):

$$N = 2^n + 2n + n_0 \quad (1)$$

where the terms are the number of FFEs (2^n), star points (2n), and zero points (n_0), respectively.

The natural and coded values of the levels for each factor are given in Table 1.

Table 1. Natural and coded values of factor levels.

Factor	Name	Dimension	Value	
			Maximum	Minimum
X_1	Photocatalyst mass	mg/50 mL	0.075	0.025
X_2	H_2O_2 volume	mL/50 mL	0.375	0.125
X_3	Processing time	min	30	10

A second-order regression model was used to describe the experimental data:

$$Y_i = \beta_0 + \sum \beta_i x_i + \sum \beta_{ii} x_i^2 + \sum \beta_{ij} x_i x_j + \varepsilon, \quad (2)$$

where β_0, β_i, and β_{ij} are coefficients for variables, and ε is a value that takes into account the influence of random factors.

The analysis of the results of the response function calculation was carried out using analysis of variance of the results.

The degree of decomposition of the pollutant was used as the response function.

$$\%X = \frac{(C_0 - C_t)}{C_0} 100\%, \quad (3)$$

where C_0 is the initial concentration of the PP in the solution, and C_t is the concentration at time t.

Identification and determination of the pollutant concentration were performed by spectrophotometric analysis.

Model calculation and subsequent optimization were performed using STATSGRAPHICS 10.0. The resulting models were tested for adequacy using the Fisher exact test, analysis of variance, and Pareto diagram analysis.

3. Results and Discussion

3.1. Composite Characterization

Figure 1a shows the X-ray diffraction pattern of the sample, synthesized in a high-pressure hydrothermal reactor. Very intense peaks of cobalt ferrite with a spinel structure are observed along the (311) plane; the peak intensity is 2000 abs units, and there are also small peaks corresponding to α-Fe.

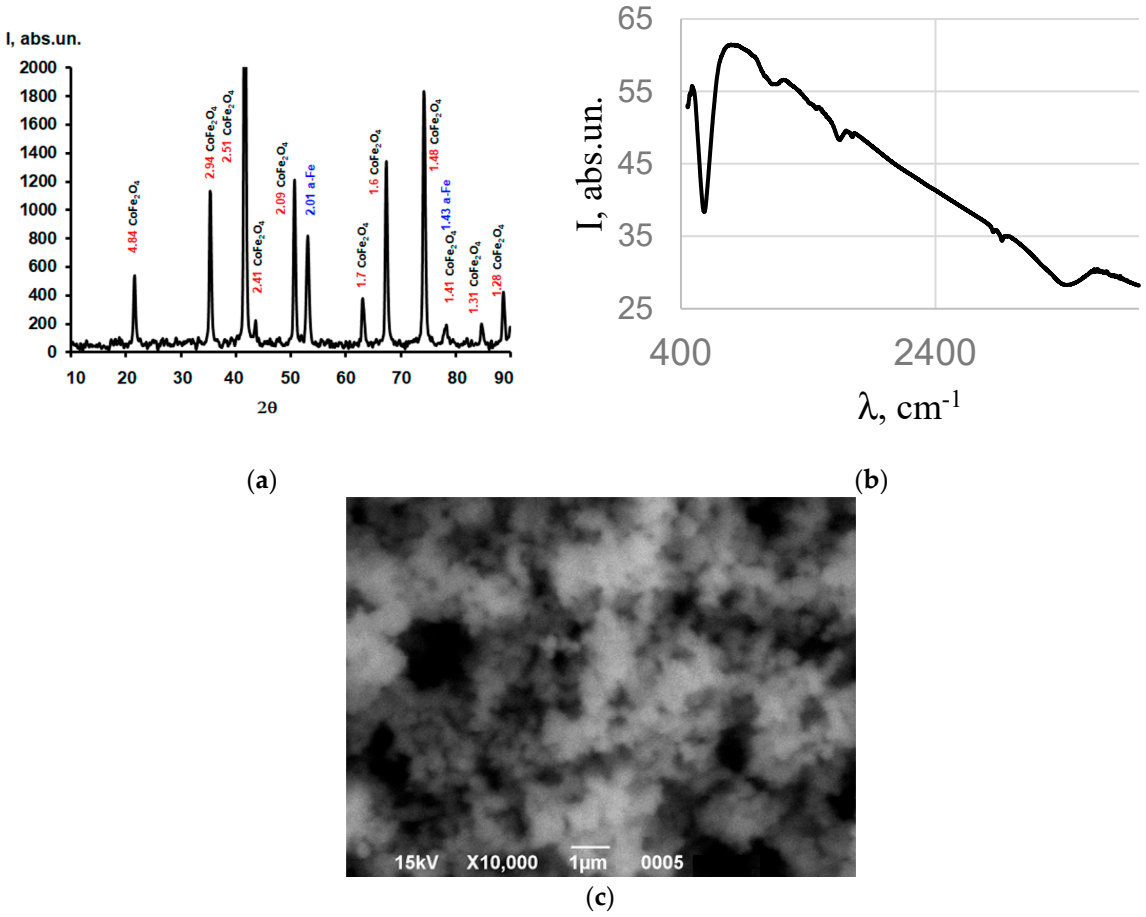

Figure 1. Composite characteristics of $Fe/CoFe_2O_4$: (**a**) X-ray pattern of the $Fe/CoFe_2O_4$ composite; (**b**) SEM image of nanoparticles of the $Fe/CoFe_2O_4$ composite; (**c**) FT-IR spectra of nanoparticles of the $Fe/CoFe_2O_4$ composite.

The X-ray diffraction data are in excellent agreement with the standard values for $CoFe_2O_4$ (JCPDS 22-1086). An anomalous increase in the crystallinity of cobalt ferrite powders obtained by hydrophase methods is observed, which is comparable with the samples obtained by sintering [25,32]. The crystallite sizes determined by different methods were L_{311} = 937 Å, L_{440} = 1041 Å, and L = 1046 Å. It should be noted that the crystallite sizes are an order larger than those obtained by, for example, the plasma method [29,35]. The crystal lattice parameter is a = 8.3901 Å and corresponds to the lattice parameter of cobalt ferrite. SEM images of the sample are shown in Figure 1c. It can be seen that the average particle size is 90–100 nm without pronounced agglomeration, which coincides with the calculated value of the crystallite size (Table 1) obtained from X-ray diffraction data. It is important to note that particle aggregation is one of the most important technological problems solved by liquid-phase technologies.

The IR Fourier spectra of the sample nanoparticles in the wavenumber range of 4000–400 cm^{-1} are shown in Figure 1b. Absorption is observed at wavenumbers of 3447, 1651, and 1124. The wavenumber of 584 cm^{-1} is characteristic and is related to vibrations

of cations in tetrahedral positions in $CoFe_2O_4$ [30,36]. The origin of the 1124 cm^{-1} band can be explained by the presence of sulfate groups, since the synthesis was carried out from iron and cobalt sulfates. It is known that the formation of hydroxo complexes often involves occlusion of the sulfate ion. A small peak at 1651 cm^{-1}, which corresponds to vibrations of absorption of water adsorbed on the surface, corresponds to the X-ray phase analysis data. The indistinct peak centered at 3447 cm^{-1} is due to stretching of the O–H bond in cobalt ferrite. The saturation magnetization of the sample is 189.24 Emu/g, which is significantly higher than that observed for cobalt ferrite (Figure 2).

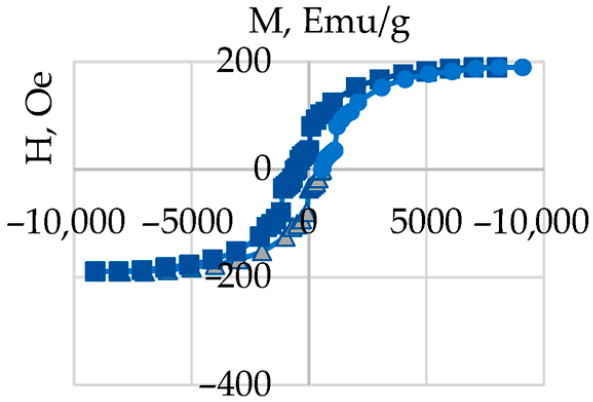

Figure 2. Magnetic hysteresis loop of the $Fe/CoFe_2O_4$ composite.

This is due to the presence of metallic iron and the formation of the $Fe/CoFe_2O_4$ composite; i.e., the presence of a ferromagnet increases the magnetic properties. The saturation magnetization value is significantly higher than the values given in [28,35]. The coercive force is 602 Oe.

Table 2 shows the main properties of the obtained composite, which characterize it as a promising material.

Table 2. Properties of the $Fe/CoFe_2O_4$ composite.

Parameters of the Sample			
No.	**Indicator**	**Explanation**	**Value**
1	L_{311}, A	Crystallite size on the 311 plane	937
2	L_{441}, A	Crystallite size on the 441 plane	1041
3	L, A	Average crystallite size	1046
4	M	Degree of microstrains	1.01×10^{-4}
5	D, cm^{-2}	Dislocation density on the 311 plane	10.45×10^{10}
6	D, cm^{-2}	Dislocation density on the 441 plane	9.21×10^{10}
7	$I_{p\ Fe}$, Abs. un.	Peak X-ray intensity	1209
8	a, A	Crystal lattice parameter	8.3901
9	Eg, eV	Gap width	2.1
10	Ms, Emu/g	Saturation magnetization	189.24
11	Hc, Oe	Coercive force	601

3.2. Investigation of the Photocatalytic Properties of the Composite

When studying the photocatalytic decomposition of pollutants, apparent rate constants of the destruction reaction in the presence of a photocatalyst were obtained with kinetic coefficients of linear regression for the zero, first, and second order of the reaction (Table 3) [36].

Table 3. Kinetic parameters for pollutant degradation.

Pollutant		Methylene Blue		Furacilin		Tetracycline		Streptocide		Ibuprofen	
Reaction Order	Equation Rate Reaction	Reaction Rate Constant	R^2	Reaction Rate Constant	R^2	Reaction Rate Constant	R^2	Reaction Rate Constant	R^2	Reaction Rate Constant	R^2
Zero	V = k	0.0163	0.59	0.065	0.953	0.085	0.77	0.042	0.92	0.0192	0.98
First	V = k[C]	0.1282	0.99	0.0374	0.986	0.347	0.99	0.022	0.98	0.0187	0.99
Second	$V = k[C]^2$	5.1321	0.64	0.1436	0.886	0.3168	0.95	0.162	0.87	0.0428	0.844

The linear plot of $\ln C/C_0$ versus t confirms a first-order reaction for PP degradation. The correlation coefficient (R^2) for the apparent first-order rate constant was close to unity.

Photocatalytic degradation occurs in pseudo-first order, and its kinetics can be expressed by the following integral relationship:

$$\mathrm{Ln}(C/C_0) = kt, \quad (4)$$

where C_0 is the initial PP concentration (mg/L), and t is the process time (min).

Analyzing the reaction rate constants given in Table 2, it is obvious that they can be arranged in order of decreasing stability as follows: ibuprofen → streptocide → furacilin → methylene blue → tetracycline. The most stable organic substance is ibuprofen, which contains a benzene ring, a carboxyl group, and a butyl radical. The presence of the benzene ring and the absence of reactive bonds makes ibuprofen and streptocide stable and persistent organic substances. Methylene blue, which has a stable aromatic structure, the heterocycle of which contains a sulfur atom and a cationic structure, is less stable and more reactive. Tetracycline contains four aromatic rings and hydroxyl groups, amido groups, and enol groups in its structure, which determines its lower stability and reactivity; however, the formation of stable intermediate compounds complicates its destruction.

3.3. Experimental Design and Photocatalytic Activity Studies

The influence of parameters such as the mass of the photocatalyst (X_1), the volume of H_2O_2 (X_2), and the time of treatment with UV radiation (X_3) on the degradation of methylene blue (MB), furatsilin (F), tetracycline (TC), streptocide (S), and ibuprofen (IF) was determined. The core of the central compositional design was a full factorial experiment (FFE) of the type with n = 3. The degree of decomposition of the substance was used as the response function.

The experiment plan consisted of 8 factor points, 6 star points, and 4 centrally repeated points, amounting to a total of 18 experiments, as shown in Table 2. Replicas in the central point allow us to estimate the error of the experiment and the adequacy of the model. The results obtained at the central point make it possible to determine the experimental mean, standard deviation, and variation of the coefficients. The response function, expressed in percentages of degradation, for each combination of factors, is shown in Table 4.

Mathematical equations obtained for the quadratic regression model are shown in Table 5.

Table 5 shows the pharmaceutical preparations under consideration in an order of increasing chemical resistance from the point of view of their structure and the possibility of formation of intermediates, as well as equations describing the degree of destruction of pollutants. All quadratic models have a high correlation coefficient that is close to unity (R^2 = 0.98–0.99), which confirms the accuracy and reproducibility of the experiments.

Table 4. Plan of central composite rotatable design for three factors and its results.

No.	m_{phot}	V_{H2O2}	τ	Xmb, %	Xfurac, %	Xibup, %	Xstrep, %	Xtetra, %
1	+1	+1	+1	98.14	98.68	73.19	90.56	76.90
2	−1	+1	+1	98.20	100.00	36.65	82.98	36.50
3	1	−1	+1	98.80	100.00	81.23	94.02	76.80
4	−1	−1	+1	99.36	81.54	58.32	83.72	63.10
5	+1	+1	−1	82.62	78.41	27.22	69.02	48.58
6	−1	+1	−1	88.66	82.92	53.40	82.73	31.38
7	1	−1	−1	92.96	78.35	41.40	83.02	42.60
8	−1	−1	−1	96.23	61.51	81.23	94.02	39.50
9	1.68	0	0	92.30	91.36	55.20	83.57	65.94
10	−1.68	0	0	96.20	79.39	57.96	86.44	37.72
11	0	1.68	0	90.10	93.65	41.52	78.82	46.22
12	0	−1.68	0	98.30	77.07	71.64	91.20	57.44
13	0	0	1.68	99.80	99.29	66.27	89.73	71.30
14	0	0	−1.68	87.22	68.90	46.89	80.29	32.36
15	0	0	0	94.50	85.30	56.58	85.01	51.83
16	0	0	0	94.70	85.68	56.58	85.01	51.83
17	0	0	0	94.40	85.30	56.58	85.01	51.83
18	0	0	0	94.80	85.68	56.58	85.01	51.83

Table 5. Statistical models describing the influence of factors on the destruction of pollutants.

No.	Pollutant	Equation	Intermediates	Name
1	Tetracycline	$X = 51.83 + 8.92m_{ad} - 3.48\ V_{H2O2} + 0.02\ V_{H2O2}^2 + 11.48\ t - 0.2\ t^2 + 5.1\ m_{ad}\ V_{H2O2} + 4.22\ m_{ad}\ t - 3.05\ V_{H2O2}\ t$	Epitetracycline (epimer at position C4) Isotetracycline, apo-tetracycline, anhydrotetracycline, epitetracycline, resistant, melanin-like polymers, organic acids [31,37]	(4S,6S,12aS)−4-(dimethylamino)−1,4,4a,5,5a,6,11,12a-octahydro−3,6,10,12,12a-pentahydroxy−6-methyl−1,11-dioxonaphthacene−2-carboxamide
2	MB	$X = 94.58 - 1.2m_{ad} - 0.03\ m_{ad}^2 - 2.45\ V_{H2O2} - 0.05\ V_{H2O2}^2 + 4.049\ t - 0.29\ t^2 - 0.28\ m_{ad}\ V_{H2O2} + 1.08\ m_{ad}\ t + 2.01\ V_{H2O2}\ t$	Leukomethylene blue, sulfoxide derivatives of phenothiazine [32,38]	3,7-Bis (dimethylamino) phenothiazin−5-ium chloride.
3	Furatsilin	$X = 85.47 + 3.56m_{ad} + 0.014\ m^2_{ad} + 4.82\ V_{H2O2} + 0.008V_{H2O2}^2 + 9.47\ t - 0.47\ t^2 - 5.25\ m_{ad}\ V_{H2O2} + 0.525m_{ad}\ t - 0.6\ V_{H2O2}\ t$	Aminofural, nitrosofural, hydrazone, organic acids [33,39]	[(E)-[(5-nitrofuran−2-yl)methylidene]amino]urea
4	Streptocide	$X = 85.22 - 0.85m_{ad} - 0.054\ m_{ad}^2 - 3.68\ V_{H2O2} - 0.054\ V_{H2O2}^2 + 2.74\ t - 0.14\ t^2 - 0.68\ m_{ad}\ V_{H2O2} + 5.32\ m_{ad}\ t + 2.63\ V_{H2O2}\ t$	Aniline, sulfamic acid [34,40]	4-aminobenzenesulfonamide
5	Ibuprofen	$X = 56.82 - 0.87m_{ad} - 0.14\ m_{ad}^2 - 8.95\ V_{H2O2} - 0.176\ V_{H2O2}^2 + 5.81\ t - 0.218\ t^2 + 3.63\ m_{ad}\ V_{H2O2} + 15.64\ m_{ad}\ t + 1.57\ V_{H2O2}\ t$	Hydroxy- and carboxy-ibuprofen [35,41]	(RS)−2-(4-(2-methylpropyl)phenyl)propanoic acid

Let us examine the influence of these factors on the degradation of methylene blue in more detail. The dependence of the degree of degradation on the above factors during UV treatment is adequately described by Equation (2) in Table 4. Figure 3a shows the Pareto

diagram constructed for the absolute values of the calculated coefficients of Equation (2). All the studied factors have a significantly smaller impact on the degree of degradation than factor x_3 (treatment time). Individual factors—photocatalyst mass and treatment time—have opposite effects. The most influential factor is treatment time. In the case of combined effects, the interaction of treatment time and peroxide concentration, as well as treatment time and photocatalyst mass, positively influences the degree of degradation.

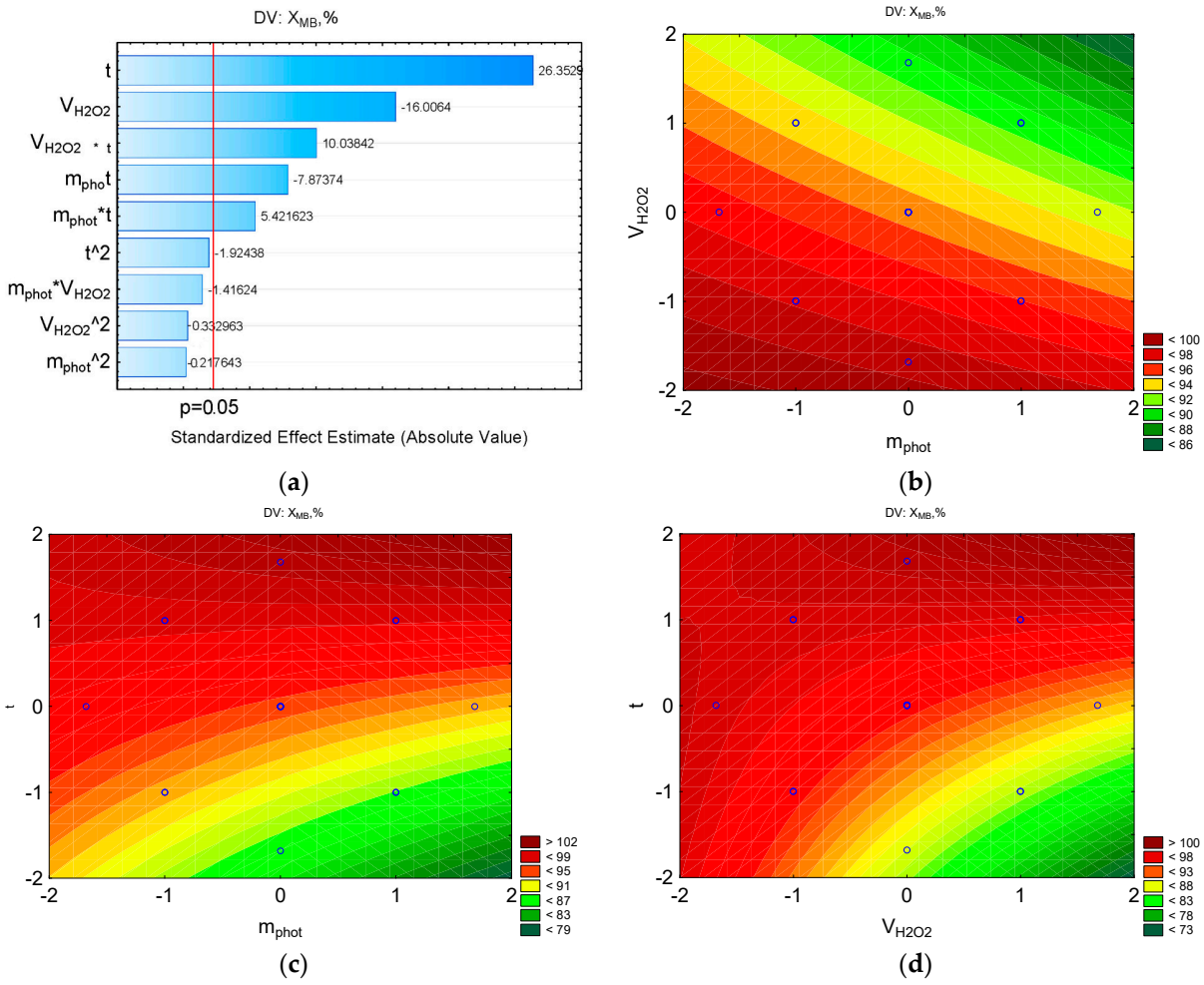

Figure 3. Counter plots showing the parameters influencing the percentage of MB to be removed: (**a**) Pareto chart to X; (**b**) X = f(V_{H2O2}, m_{phot}); (**c**) X = f(t, m_{phot}); (**d**) X = f(t, V_{H2O2}).

Figure 3b shows that the response function isolines exhibit significant curvature, with maximum values being observed at the minimum peroxide concentration and across virtually the entire range of photocatalyst mass variations. Furthermore, high degradation values correspond to combinations of 0.375 mL V(H_2O_2) and 30 min, as well as 0.125 mL V(H_2O_2) and 10 min. As seen in Figure 3c, with a 30 min treatment, a high degradation rate is achieved at a photocatalyst concentration of 0.025 g. Figure 3d shows a high degradation rate at the maximum treatment time and minimum peroxide concentration.

Analyzing all the resulting equations, it can be concluded that the degradation process of all pharmaceuticals (PPs) depends largely on the irradiation time of the solution, which significantly influences removal efficiency. Moreover, as the stability of the PP increases, the importance of irradiation time decreases, while the mass of the photocatalyst and the amount of hydrogen peroxide become more significant. The irradiation time of the solution indirectly influences the hydrolysis and dissociation of pollutants.

The influence of factors on the degradation process of tetracycline is shown in Figure 4. The influence of H_2O_2 concentration in the studied range can be assessed using Figure 4, in which it can be verified that when the concentration of H_2O_2 increased in the reaction mixture, the degree of destruction increased, but only at high photocatalyst concentrations. However, it is clear from the graph that an increase in the concentration of hydrogen peroxide in the range of 0.2–2 leads to a decrease in the degree of destruction when the solution is treated for 10–20 min (Figure 4). The data presented in the Pareto diagram in Figure 4d confirm the behavior of the H_2O_2 concentration factor, since the linear effect X_2 is significant and negative (reduces the response), and the quadratic double effect (X_2X_3) is also negative, i.e., reduces the value of the response function.

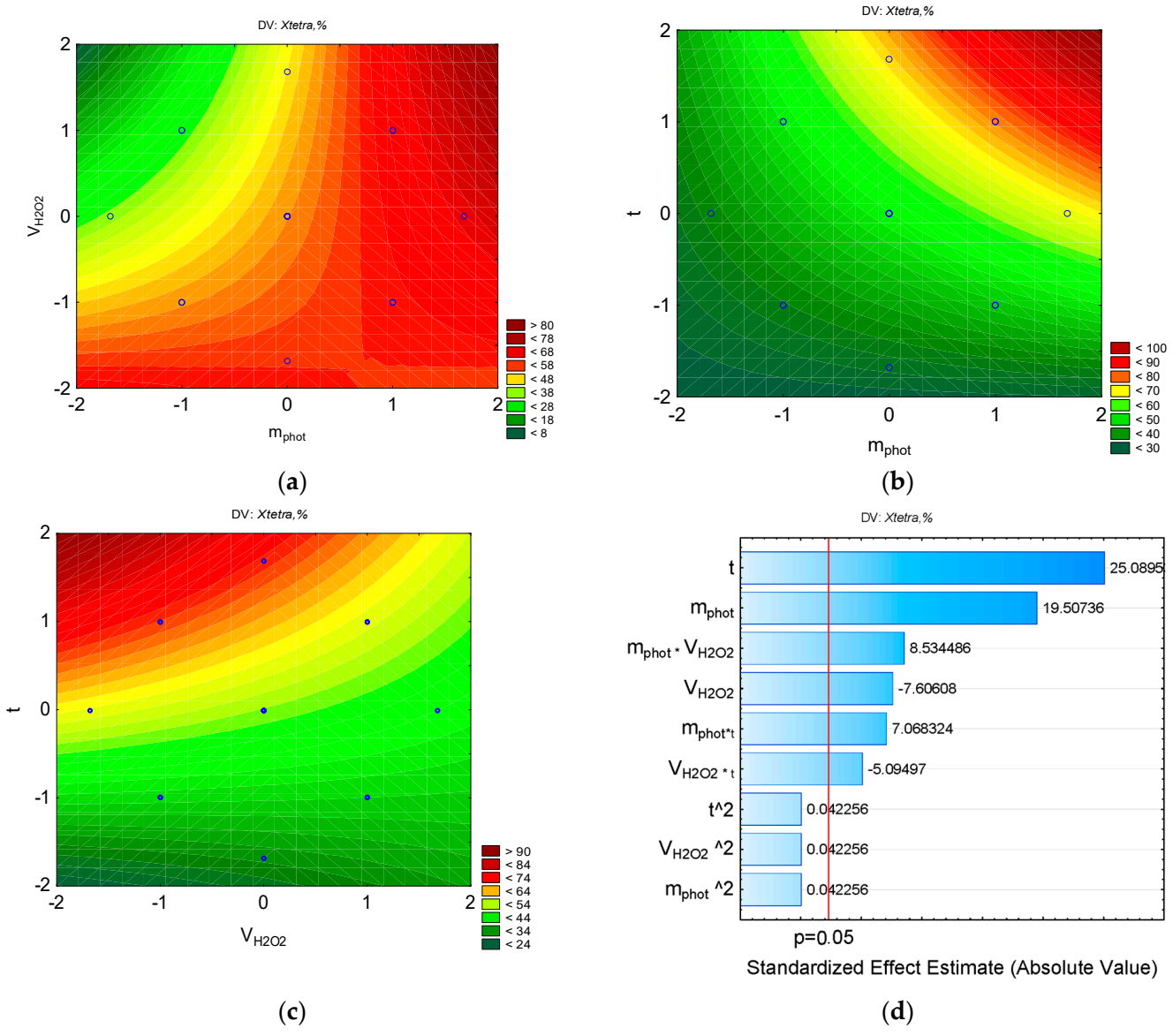

Figure 4. Counter plots showing the effects of parameters on the percent of tetracycline for removal: (**a**) X = f(V_{H2O2}, m_{phot}); (**b**) X = f(t, m_{phot}); (**c**) X = f(t, V_{H2O2}), (**d**) Pareto chart to X.

The effect of H_2O_2 concentration on the rate of furatsilin destruction in the presence of a photocatalyst is shown in Figure 5. It can be observed that the degree of destruction initially increases with increasing photocatalyst concentration at −2–0 and then decreases in the interval 1–2. Similar relationships were observed in the study of furatsilin destruction using iron and nickel oxyhydroxides [42]. The initial increase is associated with the reaction

of hydrogen peroxide with the photocatalyst with the formation of hydroxyl ions. With an excess of oxidant, hydroxyl ions recombine with the formation of products with a lower redox potential, which reduces the degree of destruction. A directly proportional relationship is observed between the concentration of photocatalyst and hydrogen peroxide: an increase in the photocatalyst content allows you to increase the peroxide concentration. Therefore, to achieve a higher rate of furatsilin degradation, the concentration of H_2O_2 should be optimal.

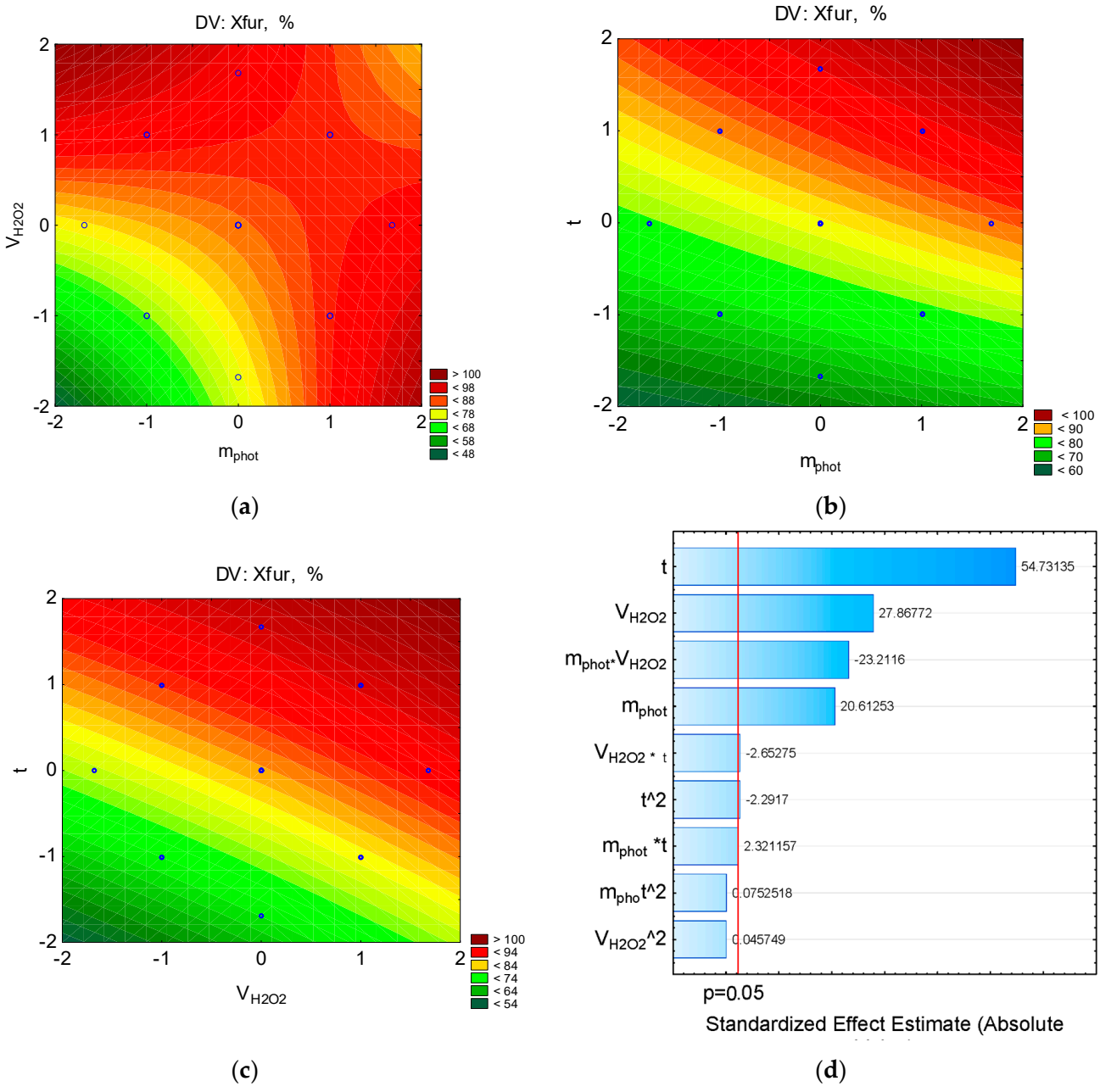

Figure 5. Counter plots showing the effects of parameters on the percent of furacilin for removal: (**a**) X = f(V_{H2O2}, m_{phot}); (**b**) X = f(t, m_{phot}); (**c**) X = f(t, V_{H2O2}) (**d**) Pareto chart to X.

Since the X = f(m_{phot}, τ) dependence for ibuprofen and streptocide has a saddle-shaped surface, it can be assumed that there is a region of metastable equilibrium, where an increase in the amount of photocatalysts can only increase the degree of destruction with an increase in the processing time, and vice versa (Figures 6 and 7). That is, competing trends are present, where maximum destruction depends on a combination of factors, and

the optimal parameters correspond to specific regions on a single line. The maximum degradation values observed at minimal peroxide concentrations, despite the change in photocatalyst mass, can be explained by the radical scavenging effect. Excess H_2O_2 inhibits the degradation reaction, as some of the radicals are consumed in the reaction with the peroxide rather than with the organic compound.

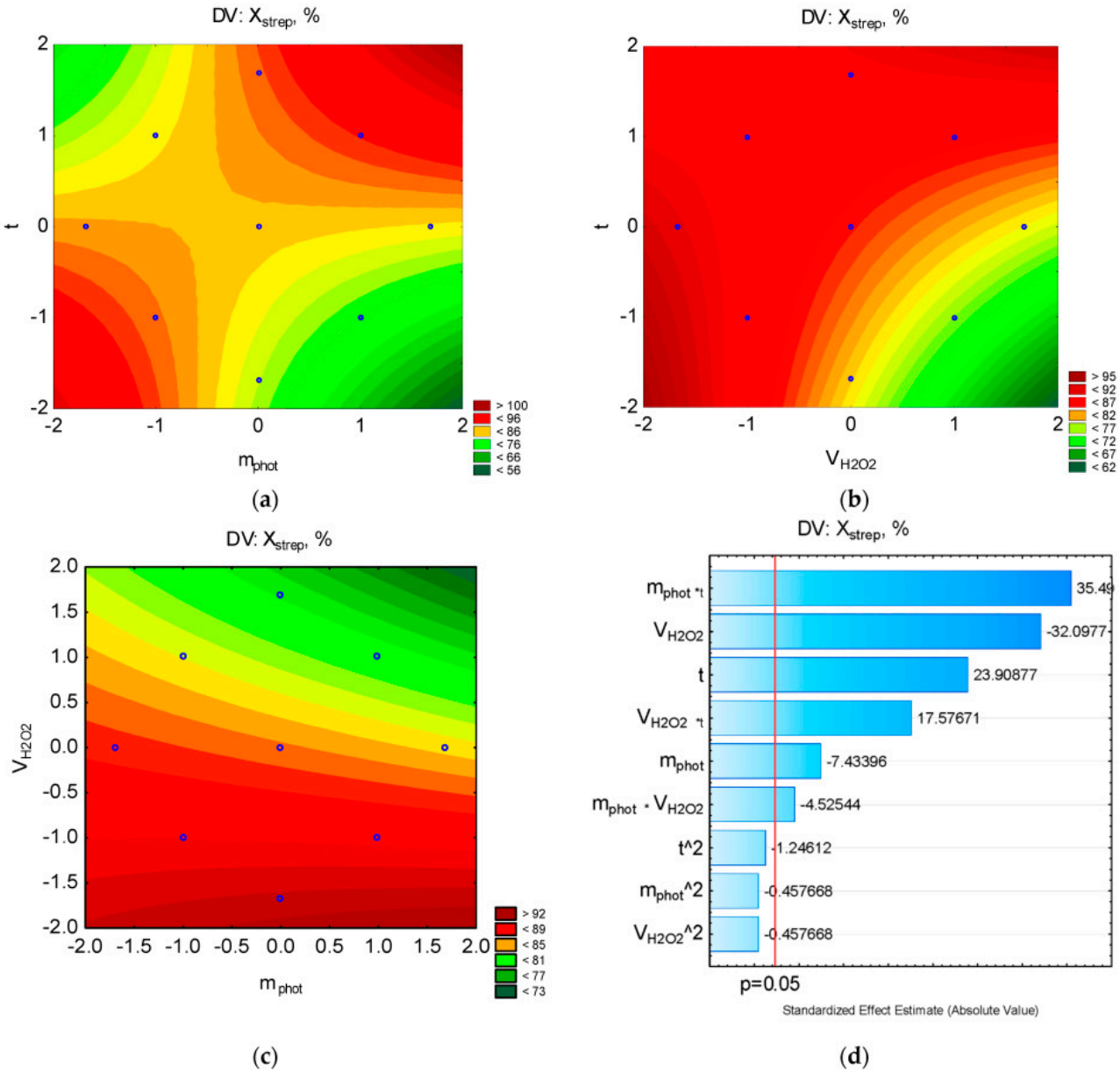

Figure 6. Counter plots showing the effects of parameters on the percent of streptocide for removal: (**a**) X = f(t, m_{phot}); (**b**) X = f(t, V_{H2O2}) (**c**) X = f(V_{H2O2}, m_{phot}); (**d**) Pareto chart to X.

As can be seen from Figures 6 and 7, the region of high X values for ibuprofen and streptocide is significantly smaller than in Figures 3–5.

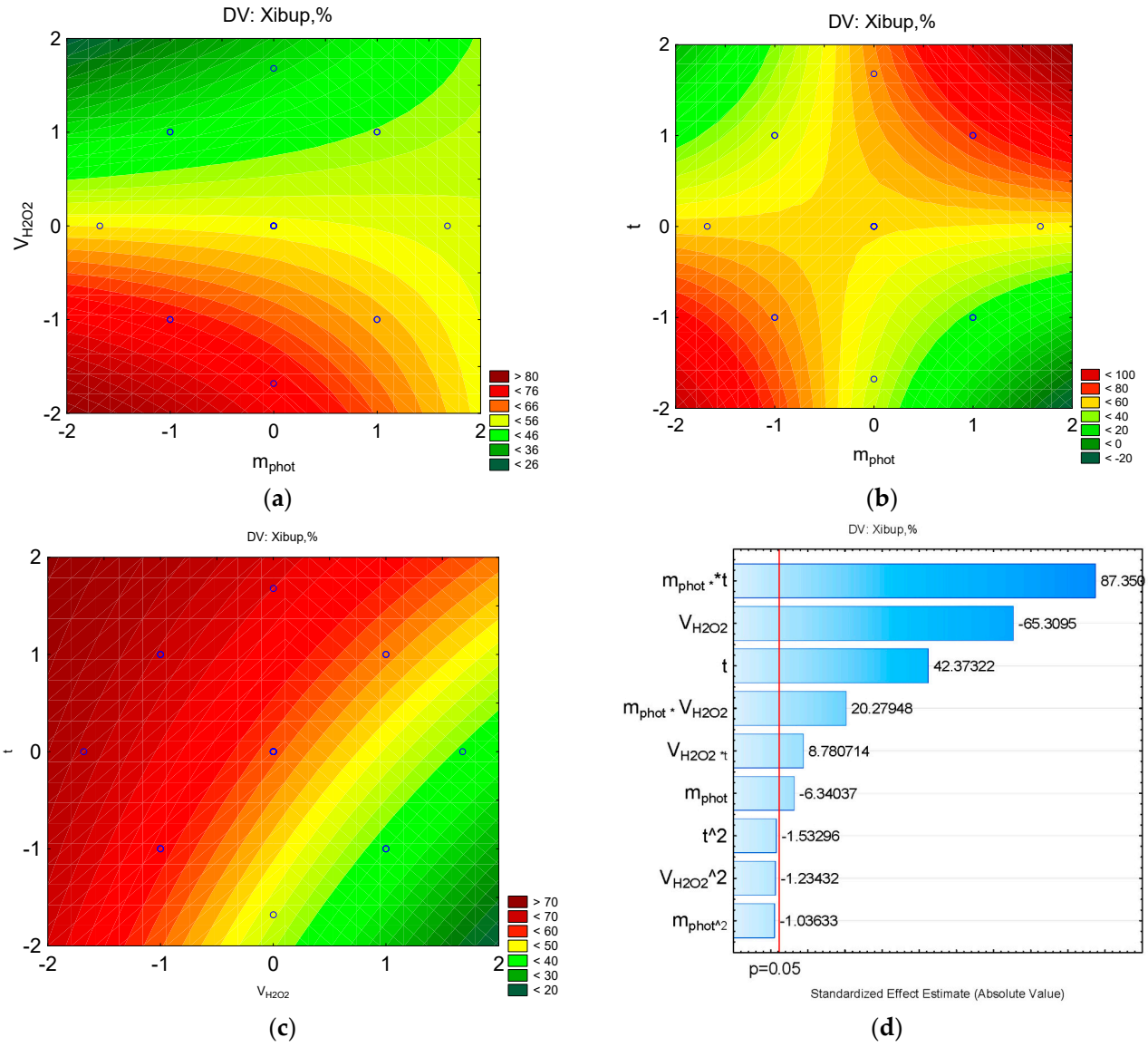

Figure 7. Counter plots showing the effects of parameters on the percent of ibuprofen for removal: (**a**) Pareto chart to X; (**b**) X = f(V_{H2O2}, m_{phot}); (**c**) X = f(t, m_{phot}); (**d**) X = f(t, V_{H2O2}).

4. Conclusions

Magnetic nanoparticles of the Fe/$CoFe_2O_4$ composite were synthesized by processing coprecipitated hydroxides and through hydrothermal treatment. The average particle size of the obtained samples, estimated by SEM microanalysis, was 90–100 nm. Magnetic properties demonstrate high saturation magnetization values of 189.24 Emu/g. The Hc value is approximately 602 Oersted. The results of studying Fe/$CoFe_2O_4$ nanocomposites demonstrate their potential as a new type of highly efficient photocatalyst in the degradation of pharmaceuticals (PPs). The main kinetic parameters of the PP degradation process were determined.

Experimental and statistical mathematical models were developed, and the largest impact factors were established. Using a different method of planning an experiment with variations in certain factors, it was possible to determine which are the most significant influxes in the process of PP degradation. It was established that during the destruction of more persistent pollutants, a consistent concentration of photocatalyst and water peroxide is important. The impact of the concentrations of water peroxide and catalyst is extreme. For more unstable PPs, the most important factor is the complexity of processing.

In addition, analysis of variance showed consistency between experimental data and theoretical values, so the mathematical models were found to be adequate.

Author Contributions: Conceptualization, L.F.; methodology, V.P.; software, V.P.; validation, T.B. and V.P.; formal analysis, T.B.; investigation, L.F. All authors have read and agreed to the published version of the manuscript.

Funding: The study was supported by the Ministry of Education and Science of Ukraine, grant No. 0124U000350.

Institutional Review Board Statement: Not applicable.

Informed Consent Statement: Not applicable.

Data Availability Statement: The original contributions presented in this study are included in the article. Further inquiries can be directed to the corresponding author.

Conflicts of Interest: The authors declare no conflicts of interest.

Abbreviations

The following abbreviations are used in this manuscript:

IR	Infrared spectrophotometer
SEM	Scanning electron microscopy
UV–visible	Ultraviolet–visible
UV	Ultraviolet
PPs	Pharmaceuticals
APIs	Active pharmaceutical ingredients
AOPs	Advanced oxidation processes
CIP	Ciprofloxacin
LEV	Levofloxacin
RhB	Rhodamine B
MWCNTs	Multiwalled carbon nanotubes
RB	Rose bengal
FFE	Full factorial experiment
MB	Methylene blue
F	Furatsilin
TC	Tetracycline
S	Streptocide
IF	Ibuprofen

References

1. O'Flynn, D.; Lawler, J.; Yusuf, A.; Parle-McDermott, A.; Harold, D.; Mc Cloughlin, T.; Holland, L.; Regan, F.; White, B. A review of pharmaceutical occurrence and pathways in the aquatic environment in the context of a changing climate and the COVID-19 pandemic. *Anal. Methods* **2021**, *13*, 575–594. [CrossRef]
2. Jurado, A.; Labad, F.; Scheiber, L.; Criollo, R.; Nikolenko, O.; Pérez, S.; Ginebreda, A. Occurrence of pharmaceuticals and risk assessment in urban groundwater. *Adv. Geosci.* **2022**, *59*, 1–7. [CrossRef]
3. Xie, H.; Hao, H.; Xu, N.; Liang, X.; Gao, D.; Xu, Y.; Gao, Y.; Tao, H.; Wong, M. Pharmaceuticals and personal care products in water, sediments, aquatic organisms, and fish feeds in the Pearl River Delta: Occurrence, distribution, potential sources, and health risk assessment. *Sci. Total. Environ.* **2019**, *659*, 230–239. [CrossRef] [PubMed]
4. Pandis, P.K.; Kalogirou, C.; Kanellou, E.; Vaitsis, C.; Savvidou, M.G.; Sourkouni, G.; Zorpas, A.A.; Argirusis, C. Key Points of Advanced Oxidation Processes (AOPs) for Wastewater, Organic Pollutants and Pharmaceutical Waste Treatment: A Mini Review. *Chemengineering.* **2022**, *6*, 8. [CrossRef]
5. Lin, Y.; Qiao, J.; Sun, Y.; Dong, H. The profound review of Fenton process: What's the next step? *J. Environ. Sci.* **2025**, *147*, 114–130. [CrossRef]
6. Ramos, M.; Santana, C.; Velloso, C.; da Silva, A.; Magalhães, F.; Aguiar, A. A review on the treatment of textile industry effluents through Fenton processes. *Process. Saf. Environ. Prot.* **2021**, *155*, 366–386. [CrossRef]

7. Çalık, Ç.; Çifçi, D.I. Comparison of kinetics and costs of Fenton and photo-Fenton processes used for the treatment of a textile industry wastewater. *J. Environ. Manag.* **2022**, *304*, 114234. [CrossRef]
8. Shokri, A.; Nasernejad, B.; Fard, M.S. Challenges and Future Roadmaps in Heterogeneous Electro-Fenton Process for Wastewater Treatment. *Water Air Soil Pollut.* **2023**, *234*, 153. [CrossRef]
9. Tanveer, R.; Yasar, A.; Tabinda, A.-U.; Ikhlaq, A.; Nissar, H.; Nizami, A.-S. Comparison of ozonation, Fenton, and photo-Fenton processes for the treatment of textile dye-bath effluents integrated with electrocoagulation. *J. Water Process. Eng.* **2022**, *46*, 102547. [CrossRef]
10. Latif, S.; Liaqat, A.; Imran, M.; Javaid, A.; Hussain, N.; Jesionowski, T.; Bilal, M. Development of zinc ferrite nanoparticles with enhanced photocatalytic performance for remediation of environmentally toxic pharmaceutical waste diclofenac sodium from wastewater. *Environ. Res.* **2022**, *216*, 114500. [CrossRef] [PubMed]
11. Gerbaldo, M.V.; Marchetti, S.G.; Elías, V.R.; Mendieta, S.N.; Crivello, M.E. Degradation of anti-inflammatory drug diclofenac using cobalt ferrite as photocatalyst. *Chem. Eng. Res. Des.* **2021**, *166*, 237–247. [CrossRef]
12. Regulska, E.; Breczko, J.; Basa, A.; Niemirowicz-Laskowska, K.; Kiszkiel-Taudul, I. Photocatalytic degradation of oxytetracycline with the REMs (Er, Tm, Yb)-doped nickel and copper aluminates. *Mater. Sci. Eng. B* **2022**, *285*, 115959. [CrossRef]
13. Niemirowicz-Laskowska, K.; Basa, A.; Breczko, J.; Kiszkiel-Taudul, I.; Wielgat, P.; Skonieczna, B.; Car, H.; Regulska, E. Sunlight-activated nanocomposites for antibiotic degradation: How $NiFe_2O_4$@TiO_2@Au tackles tigecycline and its biotoxicity. *Surf. Interfaces* **2025**, *58*, 105889. [CrossRef]
14. Breczko, J.; Basa, A.; Niemirowicz-Laskowska, K.; Skonieczna, B.; López-Martín, R.; De Toro, J.A.; Car, H.; Regulska, E. Magnetic AuNPs@TiO_2@NF heterojunction for solar-light degradation of antibiotics and mitigation of bacterial resistance risk. *RSC Adv.* **2025**, *15*, 41862–41873. [CrossRef]
15. Mohammed, N.A.H.; Shamma, R.N.; Elagroudy, S.; Adewuyi, A. Chitosan incorporated nickel ferrite photocatalyst for complete photocatalytic degradation of ciprofloxacin, ampicillin and erythromycin in water. *Results Chem.* **2024**, *7*, 101307. [CrossRef]
16. Mishra, S.; Acharya, R.; Parida, K. Spinel-Ferrite-Decorated Graphene-Based Nanocomposites for Enhanced Photocatalytic Detoxification of Organic Dyes in Aqueous Medium: A Review. *Water* **2023**, *15*, 81. [CrossRef]
17. Harikrishnan, L.; Rajaram, A. Constructive Z-scheme interfacial charge transfer of a spinel ferrite-supported g-C_3N_4 heterojunction architect for photocatalytic degradation. *J. Alloy. Compd.* **2024**, *976*, 172987. [CrossRef]
18. Ganguly, S.; Das, P.; Srinivasan, S.; Rajabzadeh, A.R.; Tang, X.S.; Margel, S. Superparamagnetic Amine-Functionalized Maghemite Nanoparticles as a Thixotropy Promoter for Hydrogels and Magnetic Field-Driven Diffusion-Controlled Drug Release. *ACS Appl. Nano Mater.* **2024**, *7*, 5272–5286. [CrossRef]
19. Stiufiuc, G.F.; Stiufiuc, R.I. Magnetic Nanoparticles: Synthesis, Characterization, and Their Use in Biomedical Field. *Appl. Sci.* **2024**, *14*, 1623. [CrossRef]
20. Aamir, M.; Aleem, W.; Akhtar, M.N.; Din, A.A.; Yasmeen, G.; Ashiq, M.N. Synthesis and characterizations of Co–Zr doped Ni ferrite/PANI nanocomposites for photocatalytic methyl orange dye degradation. *Phys. B Condens. Matter.* **2022**, *624*, 413392. [CrossRef]
21. Guo, W.; Wang, S.; Ren, Q.; Jin, Z.; Ding, Y.; Xiong, C.; Li, J.; Chen, J.; Zhu, Y.; Oh, W.-C. Microwave absorption and photocatalytic activity of MgxZn1−x ferrite/diatomite composites. *J. Korean Ceram. Soc.* **2022**, *59*, 252–262. [CrossRef]
22. Wu, Q.; Song, Y. Recent advances in spinel ferrite-based magnetic photocatalysts for efficient degradation of organic pollutants. *Water Sci. Technol.* **2023**, *87*, 1465–1495. [CrossRef]
23. Asokan, J.; Kumar, P.; Arjunan, G.; Shalini, M.G. Photocatalytic Performance of Spinel Ferrites and their Carbon-Based Composites for Environmental Pollutant Degradation. *J. Clust. Sci.* **2025**, *36*, 42. [CrossRef]
24. Mmelesi, O.K.; Ammar-Merah, S.; Nkambule, T.T.; Nkosi, B.; Liu, X.; Kefeni, K.K.; Kuvarega, A.T. The photodegradation of naproxen in an aqueous solution employing a cobalt ferrite-carbon quantum dots (CF/N-CQDs) nanocomposite, synthesized via microwave approach. *J. Water Process. Eng.* **2024**, *59*, 104968. [CrossRef]
25. Arumugham, N.; Mariappan, A.; Eswaran, J.; Daniel, S.; Kanthapazham, R.; Kathirvel, P. Nickel ferrite-based composites and its photocatalytic application—A review. *J. Hazard. Mater. Adv.* **2022**, *8*, 100156. [CrossRef]
26. Patar, S.; Mittal, R.; Yasmin, F.; Bhuyan, B.K.; Borthakur, L.J. Photocatalytic degradation of antibiotics by N-doped carbon nanoflakes-nickel ferrite composite derived from algal biomass. *Chemosphere* **2024**, *363*, 142908. [CrossRef] [PubMed]
27. Balatskiy, D.; Budnikova, Y.; Bratskaya, S.; Vasilyeva, M. TiO_2-$CoFe_2O_4$ and TiO_2-$CuFe_2O_4$ composite films: A new approach to synthesis, characterization, and optical and photocatalytic properties. *J. Compos. Sci.* **2023**, *7*, 295. [CrossRef]
28. Ahmed, A.; Alabada, R.; Usman, M.; Alothman, A.A.; Tufail, M.K.; Mohammad, S.; Ahmad, Z. Synthesis of visible-light-responsive lanthanum-doped copper ferrite/graphitic carbon nitride composites for the photocatalytic degradation of toxic organic pollutants. *Diam. Relat. Mater.* **2024**, *141*, 110630. [CrossRef]
29. Darandale, S.; Hase, D.; Mane, K.; Khedkar, J.; Murade, R.; Dichayal, S.; Murade, V. Synthesis of Spinel Ferrites and Their Composites: A Comprehensive Review on Synthesis Methods, Characterization Techniques, and Photocatalytic Applications. *J. Chem. Rev.* **2025**, *7*, 216–235.

30. Phor, L.; Malik, J.; Sharma, S.; Chaudhary, V.; Rani, G.M.; Kumar, A.; Kumar, P.; Chahal, S. Magnetically separable NiZn-ferrite/CeO2 nanorods/CNT ternary composites for photocatalytic removal of organic pollutants. *J. Mol. Liq.* **2023**, *390*, 123064. [CrossRef]
31. Singh, G.; Ubhi, M.K.; Jeet, K.; Singla, C.; Kaur, M. A Review on Impacting Parameters for Photocatalytic Degradation of Organic Effluents by Ferrites and Their Nanocomposites. *Processes* **2023**, *11*, 1727. [CrossRef]
32. Nadeem, N.; Abbas, Q.; Yaseen, M.; Jilani, A.; Zahid, M.; Iqbal, J.; Murtaza, A.; Janczarek, M.; Jesionowski, T. Coal fly ash-based copper ferrite nanocomposites as potential heterogeneous photocatalysts for wastewater remediation. *Appl. Surf. Sci.* **2021**, *565*, 150542. [CrossRef]
33. Shakirzyanov, R.; Kozlovskiy, A.; Zdorovets, M.; Zheludkevich, A.; Shlimas, D.; Abmiotka, N.; Kazantsev, P.; Zubar, T.; Trukhanov, S.; Trukhanov, A. Impact of thermobaric conditions on phase content, magnetic and electrical properties of the $CoFe_2O_4$ ceramics. *J. Alloy. Compd.* **2023**, *954*, 170083. [CrossRef]
34. Frolova, L. Photocatalytic activity of spinel ferrites $CoxFe_{3-x}O_4$ ($0.25 < x < 1$) obtained by treatment contact low-temperature non-equilibrium plasma liquors. *Appl. Nanosci.* **2020**, *10*, 4585.
35. Biswal, D.; Peeples, B.N.; Peeples, C.; Pradhan, A.K. Tuning of magnetic properties in cobalt ferrite by varying Fe^{+2} and Co^{+2} molar ratios. *J. Magn. Magn. Mater.* **2013**, *345*, 1–6. [CrossRef]
36. Atkins, P.W.; De Paula, J.; Keeler, J. *Atkins' Physical Chemistr*; Oxford University Press: Oxford, UK, 2023.
37. Bueno, M.S.; Longhi, M.R.; Garnero, C. Pharmaceutical systems as a strategy to enhance the stability of oxytetracycline hydrochloride polymorphs in solution. *Pharmaceutics* **2023**, *15*, 192. [CrossRef] [PubMed]
38. Haynes, R.K.; Chan, W.; Wong, H.; Li, K.; Wu, W.; Fan, K.; Sung, H.H.Y.; Williams, I.D.; Prosperi, D.; Melato, S.; et al. Facile Oxidation of Leucomethylene Blue and Dihydroflavins by Artemisinins: Relationship with Flavoenzyme Function and Antimalarial Mechanism of Action. *ChemMedChem* **2010**, *5*, 1282–1299. [CrossRef]
39. Bastrakov, M.; Starosotnikov, A. Recent progress in the synthesis of Drugs and bioactive molecules core. *Pharmaceuticals* **2022**, *15*, 705. [CrossRef]
40. Białk-Bielińska, A.; Stolte, S.; Matzke, M.; Fabiańska, A.; Maszkowska, J.; Kołodziejska, M.; Liberek, B.; Stepnowski, P.; Kumirska, J. Hydrolysis of sulphonamides in aqueous solutions. *J. Hazard. Mater.* **2012**, *221*, 264–274. [CrossRef]
41. Hao, H.; Wang, G.; Sun, J. Enantioselective pharmacokinetics of ibuprofen and involved mechanisms. *Drug Metab. Rev.* **2005**, *37*, 215–234. [CrossRef] [PubMed]
42. Frolova, L. H_2O_2/UV catalytic degradation of furacilin by Fe-Ni oxyhydroxides synthesized via coprecipitation. *Mater. Today Proc.* **2022**, *62*, A1–A8. [CrossRef]